Dalton Transactions

Accepted Manuscript

ROYAL SOCIETY OF CHEMISTRY

www.rsc.org/dalton

For submission to Dalton Transactions

Redox-active and DNA-binding coordination complexes of clotrimazole

Soledad Betanzos-Lara[a,+], Nikola P. Chmel[b,+], Matthew T. Zimmerman[c], Lidia R. Barrón-Sosa[a], Claudio Garino[d], Luca Salassa[e,f], Alison Rodger[b], Julia Brumaghim[c], Isabel Gracia-Mora[a], and Noráh Barba-Behrens[a,✉]

[a]Departamento de Química Inorgánica, Facultad de Química, Universidad Nacional Autónoma de México, Ciudad Universitaria, Coyoacán, México, D.F. 04510, Mexico
[b]Department of Chemistry, University of Warwick CV4 7AL Coventry, England, United Kingdom
[c]Chemistry Department, Clemson University, Clemson, SC 29634-0973, USA
[d]Department of Chemistry and NIS Centre of Excellence, University of Turin, Via P. Giuria 7, 10125 Turin, Italy
[e]CIC biomaGUNE, Paseo de Miramón 182, 20009 Donostia, Euskadi, Spain
[f]Kimika Fakultatea, Euskal Herriko Unibertsitatea and Donostia International Physics Center (DIPC), P.K. 1072, 20080 Donostia, Euskadi, Spain
[+] These two authors are equal first authors

✉Corresponding author

Tel.:+52 55 5622 3810; fax: +52 55 5616 2010

E-mail address: norah@unam.mx

Abstract DNA interactions of anticancer mononuclear Cu^{2+}, Co^{2+}, Zn^{2+}, and Ni^{2+} complexes with the biologically active ligand clotrimazole (clotri) are reported. To fully characterize DNA binding modes for these complexes of the formulae $[M(clotri)_2Cl_2]\cdot nH_2O$ (**1**–**4**), $[M(clotri)_2Br_2]\cdot nH_2O$ (**5**,**6**), $[M(clotri)_3NO_3]NO_3\cdot nH_2O$ (**9**), and $[M(clotri)_3(NO_3)_2]$ (**10**), circular dichroism (CD) and linear dichroism (LD) spectroscopy, UV melting experiments, atomic force microscopy (AFM) and ethidium bromide (EtBr) displacement methods were used. Results indicate mixed electrostatic interactions, possibly through groove binding, that result in accretion and coiling of DNA. Electrochemical studies indicate that the Cu^{2+} complex **9** readily reduces to the reactive-oxygen-species-generating Cu^{+}, which oxidatively damages DNA. There is a subtle correlation between log P values, calculated electrostatic potentials, and cytotoxicity of the complexes. The extent of cell-nucleus DNA-metal adduct formation in the HeLa cervix-uterine carcinoma cell line does not necessarily correlate with cytotoxicity, indicating that the nature of DNA lesions may be crucial to activity.

Key Words Coordination compounds · Clotrimazole · Cytotoxicity · Hydrophobicity · DNA-metal adduct · Reactive oxygen species

Introduction

Platinum complexes are the most widely used metal-based anticancer drugs [1,2]; however, new generations of agents that also possess anticancer activity but which can widen the spectrum of treatable cancers, reduce toxic side effects, and overcome resistance are needed. Multi-targeted drugs have appeared in treatment regimens as a response to this medical need given their ability to affect multiple separate biotargets [3]. One approach to developing such drugs is the use of coordination compounds bearing bioactive ligands. Some of the advantages of using the aforementioned metal complexes include their capacity to exhibit an extensive range of coordination numbers and geometries, thermodynamic/kinetic preferences for ligand atoms, and in some cases, redox activity. These properties can all exert a critical influence on the biological activity and corresponding mechanisms of action [4,5]. For example, some studies have shown that some metal ions generate reactive-oxygen-species (ROS) [6], which although being an inevitable byproduct of cellular respiration, can result in cellular and subcellular oxidative stress and in an altered homeostasis state.

In this respect, metal complexes are promising as a new generation of anticancer drugs for effective oxidant therapy; their anticancer activity may involve direct oxidative DNA-damage [7,8,9] and/or interference in the redox signaling pathways in cancer cells by novel mechanisms [10,11,12]. In particular, distortions of the DNA structure induced by metal-based anticancer agents often correlate with anticancer activity [13,14,15]. Hence, it is of great importance to understand in detail the DNA binding properties of novel metal complexes and their possible relationship to cytotoxicity in tumor cells since this may provide grounds for establishing new structure-pharmacological activity relationships. In

the studies presented herein, we demonstrate that the antitumor mechanism of mononuclear Cu^{2+}, Co^{2+}, Zn^{2+}, and Ni^{2+} complexes of the biologically active ligand clotrimazole (clotri) of the forms $[M(clotri)_2Cl_2]\cdot nH_2O$ (**1**–**4**), $[M(clotri)_2Br_2]\cdot nH_2O$ (**5**,**6**), and $[M(clotri)_3NO_3]NO_3\cdot nH_2O$ (**9**,**11**) and $[M(clotri)_3(NO_3)_2]$ (**10**) previously studied by us [17], involves not only oxidative DNA damage with generation of ROS but also specific DNA interactions.

Materials and Methods

Materials

The metal complexes were synthesized following previously described methods [16] and have been formerly reported by us [17]. Ethidium bromide (EtBr), calf thymus DNA (ct-DNA) and all the other chemicals and solvents were purchased from Sigma Aldrich and used without further purification. Synthetic B-DNA analogues were purchased from Amersham Bioscience.

Inductively Coupled Plasma Mass Spectrometry

The inductively coupled plasma mass spectrometry (ICP-MS) data where acquired on an Aurora M90 Bruker equipment. The samples were digested on a CEM MDS 2000 microwave oven using 1 mL of ultrapure HNO_3. Then, 10 mL of distilled and deionized water were added. The high-purity standards used were Cat #QCS-26 Batch # 1223440. The Blood App. Note B1-9 (App Manual CEM, Solution to sample problems CEM) was used.

Cell culture

HeLa (cervix-uterine) human carcinoma cell line was acquired from ATCC (American Tissue Culture Collection) and maintained in incubation at 310 K and 5% CO_2 with RPMI (GIBCO, Invitrogen) supplemented with 10% BFS (GIBCO, Invitrogen), 1% L-glutamine and 1% penicillin/streptomycin. Experiments were performed with cells within at least 5 passages from each other. All cells were split when around 80–95% confluence was reached using 0.25% trypsin/EDTA.

DNA-metal adduct formation

HeLa (cervix-uterine) human carcinoma cells were plated at a 3×10^6 cells/mL in two T-25 culture flasks each, provided with 5 mL of RPMI medium (GIBCO, Invitrogen) supplemented with 10% BFS (GIBCO, Invitrogen), 1% L-glutamine and 1% penicillin/streptomycin and allowed to attach at 310 K for 24 h. Next, the attached cells were released from their corresponding flasks with 2 mL trypsin-EDTA, the two suspensions put together and centrifuged at 1500 × g for 5 min. The pellet was then re-suspended in 1 mL of supplemented RPMI medium. The cells were counted and 5×10^6 cells/mL were transferred into a microcentrifuge tube and centrifuged for 5 minutes at 1500×g; the culture media was then completely removed and discarded. The pellet was then treated for DNA extraction using the Mammalian Genomic DNA Miniprep kit (G1N10, Sigma-Aldrich) following the manufacturer's procedure. All samples were stored at 253 K until ICP-MS analysis for metal content.

Determination of partition coefficient, log P

Octanol-saturated water (OSW) and water-saturated octanol (WSO) were prepared using analytical grade octanol (Sigma) and 0.3 M aqueous NaCl, NaBr, or $NaNO_3$ solutions.

Aliquots of stock solutions of the corresponding metal complexes in OSW were added to equal volumes of WSO and mixed for 4 h after partition. The aqueous and octanol layers were carefully separated into test tubes for metal analysis. Aqueous samples before and after partitioning were diluted with 2–4% HNO_3 to the appropriate range for analysis by ICP-MS calibrated with aqueous standards (Cu^{2+}, Co^{2+}, Ni^{2+}, Zn^{2+} 100.00 ± 0.5 μg/mL). These procedures were carried out at ambient temperature. Partition coefficients of M = Cu^{2+}, Co^{2+}, Ni^{2+}, Zn^{2+} complexes were calculated using the equation log P_{oct} = $\log([M]_{oct}/[M]_{aq})$.

UV-Vis absorption spectroscopy

UV-Vis spectra were recorded using a Jasco V-660 spectrometer. Circular and linear Dichroism (CD, and LD, respectively) spectra were recorded using a Jasco J-720 spectropolarimeter adapted for LD spectroscopy. All UV-Vis and CD measurements were collected in 1 cm pathlength quartz cuvettes (Starna UK). The LD measurements were performed using a quartz capillary LD Couette flow cell built by Crystal Precision Optics spinning at 3000 RPM [18,19]. CD and LD spectra were measured over the desired wavelength range using a bandwidth of 2 nm, a data pitch of 0.2 nm, scanning speed of 100 nm/min, response time of 1 s and 2 (LD) or 4 (CD) accumulations. Baseline spectra of an appropriate buffer were recorded for CD. Baseline spectra for each of the LD samples were recorded with spinning turned off. All measurements were carried out at ambient temperature.

DNA interactions

Stock solutions

All solutions of ct-DNA were prepared by dilution of 3 mM (ca. 2 mg/mL) stock solution in appropriate buffers, the exact concentrations were established using absorbance at 257 nm for ct-DNA (ε = 6600 $dm^3mol^{-1}cm^{-1}$), 254 nm for poly(dG-dC)$_2$ (ε = 8400 $dm^3mol^{-1}cm^{-1}$) and 262 nm for poly(dA-dT)$_2$ (ε = 6600 $dm^3mol^{-1}cm^{-1}$) [20,21,22]. Approximately 1 mM stock solutions of complexes **1-5** were prepared in acetonitrile, the exact concentrations were calculated assuming molecular formulas and solvents of crystallization published previously [17].

DNA melting

The stability of DNA in the presence of the metal complexes was monitored by measuring the absorbance at 260 nm as a function of temperature using the following parameters: bandwidth 2 nm, average time 10 s, heating rate 0.4 °C/min. The experiments were run simultaneously in six masked 1 cm pathlength cuvettes of 1.2 mL volume using a Peltier controlled 6-sample changer in a Jasco V-660 spectrometer. T_m (melting temperature) was calculated within the thermal heating program by applying a first derivative calculation. The concentration of ct-DNA was 7.5×10^{-5} M (per base) and buffer conditions were 10 mM Tris buffer (pH 7.0) and 1 mM EDTA in 50% acetonitrile.

Ethidium Bromide (EtBr) displacement assay

Fluorescence measurements were performed at ambient temperature on a Jasco FP-6500 spectrofluorophotometer using a 0.5 cm path length quartz cell. The DNA–EtBr complexes were excited at 546 nm and the fluorescence was measured at 585 nm. Aliquots of a 1 mM stock solution of the compound in acetonitrile were added to a solution of EtBr and DNA (10 mM Tris pH 7.0, 1 mM EDTA, 1.3 μM EtBr, and 3.9 mM DNA in 10% acetonitrile).

Concentrations of DNA and EtBr were kept constant by addition of an equal volume of EtBr or DNA solution at double the concentration. The fluorescence was measured after each addition until the signal was reduced by 50%.

Circular dichroism (CD) titrations

Starting solutions of 50 μM DNA in 1 mM Tris (pH 7.0), 0.1 mM EDTA, and 50% acetonitrile buffer were titrated with 0.1 and 1 mM stock solutions of the clotri metal complexes in acetonitrile. Concentrations of DNA and acetonitrile were kept constant throughout the titration by addition of an equal volume of 100 μM DNA solution. Concentration of the compound was increased from 0 to 50 μM.

Linear dichroism (LD) titrations

Due to the small volume of sample used in a typical experiment (60 μL) each sample in the titration series was prepared separately. All solutions were prepared in 10 mM Tris (pH 7.0), 1 mM EDTA, 50% acetonitrile buffer. The ct-DNA concentration was kept constant throughout the experiment at 100 μM, and the compound concentration was increased from 0 to 100 μM. Acetonitrile concentration was kept constant at 50%.

Electrochemistry

Cyclic voltammetry (CV) and differential pulse voltammetry (DPV) experiments were conducted with a CH Electrochemical Analyzer (CH Instruments, Inc.) in dry, degassed acetonitrile (or dichloromethane) with tetra-*n*-butylammonium hexafulrophosphate (100 mM) as a supporting electrolyte. The final concentrations of all compounds were 1 mM, with a final volume of 5 mL. All samples were degassed for 10 min with N_2 before each

experiment. CV experiments were conducted with a scan rate of 100 mV/s, and all figures show the overlay of the second and third scans. DPV experiments were conducted on all samples (some data not shown) and confirmed all waves observed in the cyclic voltammograms. Due to limited solubility, some of the compounds precipitated slightly towards the end of the electrochemical measurements in all solvents. All voltammograms were reproducible even when precipitation occurred. A pulse amplitude of 0.020 V and a pulse width of 0.050 were used for all DPV experiments, in conjunction with a sample width of 0.020 and a pulse period of 0.100. Samples of each complex were cycled between −1.6 V and 1.6 V using a glassy carbon working electrode, a Pt counter electrode, and a Ag/AgCl (+0.197 V vs. NHE) [23] reference electrode. All experiments were externally referenced to ferrocene (0.593 V vs. Ag/AgCl) [24].

DNA damage gel electrophoresis

Deionized water, MOPS buffer (10 mM, pH 7.39), NaCl (130 mM), ethanol (10 mM), ascorbate (1.25 equivalents per Cu^{II} ion; 7.5-62.5 μM), and the indicated concentrations of the Cu^{2+} complex (1-50 μM) in water were combined in a microcentrifuge tube and allowed to stand for 5 min at ambient temperature. Plasmid DNA (pBSSK; 0.1 pmol in 130 mmol NaCl solution) was then added to the reaction mixture and allowed to stand for 5 min at ambient temperature. Hydrogen peroxide (50 μM) was added and allowed to react at ambient temperature for 30 min, and then EDTA (50 μM) was added to quench the reaction. All given concentrations are final concentrations in a 10 μL volume. Samples were loaded into a 1% agarose gel in TAE running buffer; and damaged and undamaged plasmid DNA were separated by electrophoresis (140 V for 30 min). Gels were then stained using EtBr and imaged under UV light. The amounts of nicked (damaged) and circular

(undamaged) DNA were quantified using UViProMW (Jencons Scientific Inc., 2007). The intensity of the circular plasmid band was multiplied by 1.24, due to the different binding abilities of EtBr to supercoiled and nicked plasmid DNA [25,26].

Atomic Force Microscopy (AFM) imaging

Mica was purchased from Agar Scientific and was freshly cleaved before use using Sellotape. AFM images were recorded in tapping mode on Veeco Multimode V using Bruker FMV silicon probes (average resonant frequency 75 kHz, nominal spring constant 2.8 N/m). Recorded images were processed using WSxM software [27]. pUC19 plasmid was purchased from New England Biolabs, Hind III enzyme was purchased from Invitrogen. pUC19 plasmid DNA (2686 bp) was linearized using Hind III enzyme following the recommended manufacturer procedure. The reaction mixture was purified using QIAprep Spin Miniprep Kit following the manufacturer procedure. The concentration of the obtained linear DNA was determined using absorbance at 260 nm. Solutions of linearized plasmid DNA (11 μM) with appropriate concentrations of the compound in 5 mM $MgCl_2$/2.5% acetonitrile were prepared and left to equilibrate for 20 min at ambient temperature. 1 μL of the solution was then deposited for 10 min on a freshly cleaved surface of mica. The mica surface was subsequently washed for about 2 to 3 s with a jet of deionized water from a wash bottle and dried under a stream of nitrogen.

Computational details

Calculations on complexes **1**–**7** were performed with the Gaussian 09 program [28], employing the DFT method with the PBE0 functional [29]. The LanL2DZ effective core potential [30] was used for the Cu, Co, Zn and Ni atoms and the 6-31G** basis set [31] was

used for all other atoms. Geometry optimizations were performed using the PCM method [32] and water as solvent. The nature of the stationary points was confirmed by normal mode analysis. Electrostatic potential surfaces (EPS) are shown both in space and mapped on electron density (isovalue 0.001) of the molecules. The electrostatic potential is represented with a color scale going from red (–0.1 a.u.) to blue (0.1 a.u.).

Results and Discussion

Structural properties of complexes 1–7

To characterize the structural features of the clotri derivatives investigated in this work (Figure 1), Density Functional Theory (DFT) geometry optimization calculations on complexes **1**–**7** were performed at the PBE0/LanL2DZ/6-31G** level [29,30,31] using the PCM [32] method for including solvent (water) effects. Details are summarized in Table 1. In the case of **3** and **7**, their X-ray structures were previously solved [17] and the calculated geometries display a good agreement with them, although bond distances and angles are somewhat overestimated by calculations as demonstrated previously for other systems [33]. Cu^{2+} and Co^{2+} derivatives were optimized as doublets and quartets respectively, while Zn^{2+} and Ni^{2+} were optimized as closed-shell complexes [34].

Complexes **1**–**7** adopt a pseudo-tetrahedral coordination environment with both chlorido and bromido ligands in a *trans*-like geometry. This conformation was found to be the most stable compared to the *cis*-like structure (ΔE = 3.06–7.40 kJ/mol). In complexes **1**–**4**, M–Cl bond distances are in the range of 2.357–2.323 Å and are very similar to each other despite the differences in the central metal ions. An analogous trend was observed for the M–Br

bonds in complexes **5**–**7**, although at slightly larger values as expected. M–$N_{(clotri)}$ distances are comparable for all complexes, and the Cu^{2+} derivatives **1** and **5** have the smallest values. The electrostatic potential surfaces (EPS; Figure 2 and Figure S1) show that complexes **1**–**4** and **5**–**7** have a similar charge distribution.

Partition Coefficient (log P values)

It is known that the ability of a given drug to permeate biological membranes depends strongly on its lipophilicity [35], which is commonly experimentally determined by the partition coefficient of the compound in *n*-octanol/water ($P_{o/w}$) [36]. Lipophilicity has been shown to affect absorption, transmembrane transport by means of passive diffusion reflecting the relative solubility of the drug in lipid-like (i.e. lipid bilayers of a cell membrane) and aqueous (the fluid in and out of cells) environments, bioavailability, cellular drug accumulation, hydrophobic drug-receptor interactions, metabolism, pharmacological activity, and toxicity of molecules [37]. It has been previously reported that reduced uptake, resulting from either increased efflux or reduced influx, contributes to the acquired cisplatin resistance of tumors [38,39,40]. In general terms, for an effective anticancer drug to initiate cell death, it must reach all viable cells in a tumor and be retained in sufficient concentrations on a relevant time scale. The partition coefficient (log P) values for the Cu^{2+}, Co^{2+}, Zn^{2+}, and Ni^{2+} clotri complexes are shown in Table 2. The values that range from –2.09 to –0.27 do not necessarily correlate with cytotoxicity, and are significantly higher than that of cisplatin (–2.30) [41].

DNA melting

Due to the low solubility of some of these compounds in buffer solutions, most of the samples used in the measurements contained a significant fraction of acetonitrile (up to 50%). We have, however, shown previously that even high acetonitrile contents (≤60%) do not noticeably alter the structure and activity of B-DNA [42].

DNA melting temperature (T_m), defined as the temperature at which half of the DNA double strands are unwound into single strands, is an effective measure of thermal stability of DNA and DNA adducts [43]. DNA is believed to be a binding target for the clotrimazole metal complexes studied here, and this binding may result in the observed cytotoxicity [17]. To determine if binding of these clotri complexes affects the stability of DNA structure, the melting temperatures of ct-DNA in the absence and presence of different concentrations of the metal compounds **1**–**3** and **9**–**10** as representative examples, were determined. The results obtained are summarized in Figure 3. All compounds affect only very small changes on the thermal stability of DNA, near the detection limits of the instrument, as evidenced by the error bars. At all tested concentrations, compounds **1** and **10** show no effect on thermal stability of DNA, whereas compounds **2**, **3** and **9** lower the melting temperature of ct-DNA by approximately 0.5 °C. In all the cases, there is no significant change in melting temperature as the concentration of the compound is increased. These results suggest that DNA binding, if any, is quite weak and it does not significantly affect its thermal stability. Thus, weak electrostatic forces may be pointed as the main mechanism of interaction.

Ethidium bromide (EtBr) competition assay

Ethidium bromide displacement experiments allow quantification of binding constants for DNA-binding compounds in relation to that of EtBr [44]. EtBr is a known intercalator,

binding between the stacked base pairs of the DNA with its long axis parallel to the long axis of the base pairs) [45]. Upon DNA binding, EtBr exhibits strong fluorescence that can be used to monitor the binding process. To extract more information about the DNA-binding of the selected clotri metal complexes and the possible sequence specificity, three different B-DNA analogs, including ct-DNA, poly(dA-aT)$_2$, and poly(dG-dC)$_2$, were used. A typical titration curve is shown in Figure 4 for complex [Cu(clotri)$_2$Cl$_2$]·5H$_2$O (**1**), the inset shows decreasing intensity of EtBr fluorescence at 585 nm. The apparent binding constants (K_{app}) were calculated using formula: $K_{app} = \frac{c}{K_{EtBr}[\mathbf{EtBr}]}$ where c is the concentration of the compound at 50% observed reduction in fluorescence, [EtBr] is the concentration of ethidium bromide and K_{EtBr} is known (K_{EtBr} = 1 × 10^7 M^{-1} for ct-DNA, 9.5 × 10^6 M^{-1} for poly(dA-dT)$_2$ and 9.9 × 10^6 M^{-1} for poly(dG-dC)$_2$) [44]. The calculated K_{app} values for compounds **1**–**3** and **9**–**10** are shown in Table 3. For ct-DNA, compounds **1**–**3** show very similar K_{app} values of approximately 4.8 × 10^4 M^{-1}. Similarly, compounds **9** and **10** show similar K_{app} values approximately 1.5 times higher (ca. 6.5 × 10^4 M^{-1}). For comparison, the binding constant (K_{app}) of EtBr under the same conditions is on the order of 10^6 M^{-1} [46]. Excellent agreement between the three values obtained for the bis-ligand compounds and the two higher values obtained for tris-ligand complexes suggests that DNA binding of these species is ligand-dependent and that the nature of the central atom might be of a secondary significance for the binding process. The situation, however, changes for metal complex binding to synthetic poly(dA-dT)$_2$ and poly(dG-dC)$_2$ B-DNA analogues. All of the compounds show a generally higher preference for binding poly(dG-dC)$_2$. In the case of poly(dA-dT)$_2$, bis-ligand complexes show higher binding constants compared to those for ct-DNA, whereas tris-ligand compounds show lower K_{app} values

compared to those for ct-DNA. This suggests that a second sequence selective binding mode is available for these compounds in addition to the non-specific electrostatic binding. This more selective mode becomes apparent in binding to synthetic DNA analogues. All of the compounds exhibit slight preference for guanine-cytosine (GC) motifs. The apparent binding constants to synthetic DNAs for compounds **1**, **9** and **10** are very similar, ca. 6.3×10^4 M^{-1} for poly(dA-dT)$_2$ and 6.6×10^4 M^{-1} for poly(dG-dC)$_2$. Compounds **2** and **3** show significantly lower apparent binding constants for both poly(dA-dT)$_2$ and poly(dG-dC)$_2$ DNA, suggesting that, in contrast to binding observed previously for ct-DNA, this binding mode is largely independent on the number of ligands. It is worth noting that all the tested compounds exhibit weak fluorescence at approximately 310 nm. Due to the characteristics of the grating monochromator, this emission was also visible at 620 nm (Figure 4) and may have contributed to higher errors for some measurements as especially evident in the case of Co^{2+} clotri complexes (**2** and **10**) upon binding to poly(dG-dC)$_2$.

Linear Dichroism

Linear dichroism (LD) is the difference in absorption of parallel and perpendicular linearly polarized light in an aligned sample [47]. LD is an especially convenient method to probe DNA binding due to the linear nature of the DNA molecule. A DNA solution is aligned using the laminar flow between two concentric cylinders, one of which is stationary and the other of which is rotating at approximately 3000 RPM [18,19,47]. Small molecules that are not aligned under these conditions are not visible in LD, and only large and linear structures such as DNA give rise to LD signals. Upon binding to DNA, small molecules become aligned and can give rise to new LD signals. Sign and magnitude of these signals often allows for determination of relative orientation of the binding species and thus the binding

mode [48]. An LD titration of ct-DNA and complex $[Cu(clotri)_2Cl_2]\cdot 5H_2O$ (**1**), and the resulting titration curve are shown in Figure 5. Data for the compounds **2**, **3**, **9** and **10** can be found in the supplementary information (Figures S2-S5). Due to weak absorbance of compounds **1–3** and **9**-**10** in the visible part of the spectrum, no additional LD peaks were observed in this region.

In the UV range, emergence of weak signals was observed at high compound concentrations, but these are mainly obscured by the strong DNA signals in those regions. To estimate the induced LD behavior of complex $[Cu(clotri)_2Cl_2]\cdot 5H_2O$ (**1**), a ct-DNA spectrum was overlaid on a spectrum of ct-DNA with 50 μM of **1** and scaled to the same intensity at 247 and 350 nm (weak or no absorbance of the compound). The differential spectrum was then calculated (Figure 6, right) and a UV spectrum of **1** was overlaid for comparison. There is a reasonably good agreement between the shape and the positions of the main bands in both the calculated LD spectrum and the UV spectrum, suggesting that the new bands are indeed caused by binding of the compound. The presence of new LD signals demonstrates that **1** binds to the DNA in an oriented fashion (i.e., groove binding or intercalation). A non-specific binding mode (i.e., electrostatic interactions) would not result in such an alignment. The structure of the clotri complexes makes intercalation a relatively unlikely mode of binding, which is supported by the presence of weak positive signals in the calculated LD spectrum (195 nm). For intercalation, generally only negative signals would be expected, indicating that **1** is most likely a groove binder. Similar patterns of signals were detected in all the tested compounds (data available in the SI Figures S6-S9), suggesting that one binding modes for all these compounds is groove binding.

In all the titrations, the intensity of the strong negative signal from the π-π* transitions in the DNA base pairs at 260 nm decreased in magnitude upon increasing concentrations of the compound. This phenomenon results from effective shortening of DNA strands due to bending, kinking, or aggregation upon binding [49], lowering the linearity of DNA and thus its alignment with the flow. It has previously been demonstrated that, in extreme cases, B-DNA strands can coil into small bundles, resulting in complete loss of negative signal at 260 nm [49]. CD results rule out formation of kinks as the cause of DNA shortening, leaving bending as the most likely cause. This is further supported by the AFM images (*vide infra*).

To compare the relative effects of these complexes on DNA coiling, the titration curves were fitted to the Hill equation, and the concentration of ligand at which 50% loss of LD signal (K_a) was calculated (Table 4). As previously described, there is no obvious relation between these values and the structures of the compounds. Generally, the K_a value increases (activity towards DNA decreases) in the series Cu^{2+}, Zn^{2+}, and Co^{2+}, with bis-ligand complexes showing smaller K_a values compared to the tris-complex of the same metal. The K_a values obtained for the Co^{2+} complexes (**2** and **10**) show significantly higher values (lower DNA activity) compared to others. Interestingly, in the case of **2** and **10**, two distinct stages can be identified on the titration curve. At low concentrations, the LD signal seems to follow a typical saturation curve, with a second step at higher concentrations (Figure 7). This directly supports the previous evidence of at least two possible binding modes. Competition between binding modes for the cobalt complexes may also explain the relatively high errors obtained for these compounds in the EtBr displacement assay.

Circular dichroism

To determine if DNA binding of the clotri metal complexes causes changes in the helical structure of B-DNA, CD spectra of DNA with increasing concentrations of compounds **1**–**3** and **9**–**10** were acquired. As in the LD experiments, DNA concentration was kept constant throughout the titration by addition of equal volumes of double concentrated stock solution. In all cases, no significant changes were observed in a wide range of concentrations. Upon increasing the concentration of the compound to approximately 50 μM (1:1 complex:DNA ratio) a small decrease in the CD magnitude was observed. Figure 8 shows the CD spectra for $[Zn(clotri)_2Cl_2]$ (**3**), and data for the other compounds are available in the SI (Figures S10-S13). In all cases, only very small changes are observed in the CD spectra at the same concentration range that shows very large changes in the LD. Thus, binding of these complexes affects DNA alignment (bending or kinking), but it does not significantly affect the B-DNA helical structure. This strongly suggests that the shortening of DNA observed in the LD is most likely caused by bending, since kinking would be expected to cause considerable distortion that would be easily observable in CD [50].

Atomic Force Microscopy (AFM) imaging

To understand the cause of the loss of DNA signal in the LD spectra upon metal complex binding, a series of tapping mode atomic force microscopy (TM-AFM) images of linearized plasmid DNA (pUC19, 2686 bp) were recorded with increasing concentrations of $[Cu(clotri)_2Cl_2]\cdot 5H_2O$ (**1**). The non-covalent binding of metal complexes causes different effects on DNA tertiary structure, including inter- and intra-molecular coiling [49,15]. For both DNA alone and with low concentrations of **1** (Figure 9A and B), the DNA strands are well separated with little evidence of coiling, consistent with CD and LD results. At high DNA:compound **1** ratios (10:5; Figure 9D), no linear DNA was detected on the mica

surface, only various-sized aggregates large enough to be formed from more than one DNA strand. Several attempts were made to record an image in which both aggregates and linear DNA were present, and the best result is shown in Figure 9C. The difficulty in recording such an image indicates the very high cooperativity of this process. At moderate concentrations of **1**, a much higher inter-connectivity between the DNA strands is observed, as well as early evidence of tight coiling, consistent with results obtained by other methods. At low concentrations, the interaction of **1** with DNA is weak and does not induce changes in the DNA tertiary structure, but at moderate and high concentrations, a mixture of electrostatic interactions and possibly groove binding results in accretion and coiling of the DNA strands into tightly wound aggregates.

Electrochemistry

Electrochemical studies of the unbound clotri ligand show that it is redox inactive within the investigated window (Figure S14A). $[Zn(clotri)_2Cl_2]$ (**3**) and $[Zn(clotri)_3NO_3]NO_3{\cdot}5H_2O$ (**11**) (cyclic voltammograms in Figures S14B and S14D, respectively) also exhibit no electrochemical activity. In contrast, similar studies of $[Zn(clotri)_2Br_2]$ (**7**), Table 5 and Figure S14C, show clotri-based redox waves with an $E_{1/2}$ potential of 0.806 V, indicating that metal coordination shifts these ligand-based potentials into the measureable electrochemical window. These results are in agreement with DFT frontier orbital calculations (Figure S15) and with previous studies of metal-coordinated histidine and imidazole-derived ligands [51,52]. For all three complexes, the Zn^{2+} center is electrochemically inactive within the examined potential window. The cyclic voltammogram of $[Co(clotri)_2Cl_2]$ (**2**) in Figure S16 exhibits an anodic wave at 1.206 V due to clotri ligand oxidation, whereas anodic waves at 0.977 V and -0.238 V represent $Co^{2+/3+}$

and $Co^{0/2+}$ oxidations, respectively (Table 5). Similar redox behavior for $[Co(clotri)_2Br_2]$ (**6**) is observed (Figure S17B) and DFT frontier orbital calculations for complex **6** support the electrochemical assignments (Figure S15).

Differential pulse voltammetry (DPV) studies confirm the presence of clotri ligand oxidation and reduction waves for both complex **2** ($E_{1/2}$ = 1.111 V; Figures S17A and S17B) and complex **6**, as well as unambiguously identifying the clotri reduction wave for complex **6** (Figures S17C and S17D). DPV-derived potentials are not included in Table 5, since they are typically shifted compared to CV potentials [53,54]. The CV of the nitrate complex, $[Co(clotri)_3(NO_3)_2]$ (**10**), exhibits only a $Co^{2+/0}$ redox couple with an $E_{1/2}$ value of –0.982 V. DPV studies of the nitrate complex also show redox potentials for the $Co^{3+/2+}$ couple and the clotri ligand (Figures S18A and S18B). The more positive Ep_a value for the $Co^{2+/3+}$ oxidation of $[Co(clotri)_2Cl_2]$ (**2**) compared to $[Co(clotri)_2Br_2]$ (**6**) indicates that chloride coordination stabilizes Co^{3+} over Co^{2+} compared to bromide coordination. Previous studies [51] of dichloride and dibromide Co^{2+} complexes with a three-nitrogen-donor, conjugated bis(imino)pyridine ligand showed a similar Co^{3+} stabilization ($E_{1/2}$ values of 0.153 and -0.087 V, respectively).

The Cu^{2+} complex $[Cu(clotri)_2Cl_2]\cdot 5H_2O$ (**1**) exhibits both quasi-reversible $Cu^{2+/+}$ and $Cu^{+/0}$ redox couples with $E_{1/2}$ values of -0.239 and -0.852 V, respectively (Figure 10). The CV of $[Cu(clotri)_2Br_2]\cdot 5H_2O$ (**5**) in Figure 10B, also shows $Cu^{2+/+}$ and $Cu^{0/+}$ redox couples ($E_{1/2}$ = -0.139 and -1.022 V, respectively) as well as clotri redox activity ($E_{1/2}$ = 0.788 V; Table 5), despite precipitation during the experiment. DFT frontier orbital calculations for complex **5** support such assignments, Figure S15. The anodic wave around 0.190 V and the cathodic wave around 0.620 V may result from formation of an electrochemically active acetonitrile

complex upon decomposition of the complex [55]. Because complexes **1** and **5** precipitated during the CV experiments in acetonitrile and made the electrochemical waves difficult to detect, similar studies were conducted in CH_2Cl_2 to confirm these results (Table S1). $[Cu(clotri)_3(NO_3)]NO_3 \cdot 2H_2O$ (**9**) remained in acetonitrile solution and exhibits a strong, quasi-reversible $Cu^{+/0}$ reduction potential ($E_{1/2}$ = -1.022) and two weaker quasi-reversible reduction potentials for $Cu^{2+/+}$ and the clotri ligand ($E_{1/2}$ values of -0.012 V and 0.515 V, respectively; Table 5).

The $Cu^{2+/+}$ reduction potential of the chloride complex is the most negative, followed by the bromide and nitrate complexes, indicating that the hard chloride ligands most stabilize Cu^{2+} relative to Cu^{+} and consistent with the trend observed for Co-clotri complexes. Based on the electrochemical potentials, the additional borderline clotri ligand present in nitrate complex **9** has a greater influence on Cu^{2+} stability than the hard nitrate ligand. Electrochemical studies of $[CuCl(tptm)]^{+}$ and $[CuBr(tptm)]^{+}$ (tptm = tris(2-pyridylthio)methyl) also reported a decrease in $Cu^{+/2+}$ oxidation potential for analogous chloride and bromide complexes (Ep_a values of -0.560 and -0.463 V, respectively) [56].

Oxidative DNA damage

Gel electrophoresis studies were performed on $[Cu(clotri)_3(NO_3)]NO_3 \cdot 2H_2O$ (**9**) to determine its ability to promote oxidative DNA damage caused by Cu^{+}/H_2O_2 (pH 7). Ascorbic acid (1.25 equiv) was added to the Cu^{2+} complex to reduce Cu^{2+} to hydroxyl-radical-generating Cu^{+} (equation 1) [57] and ethanol (10 mM) was added as a well-studied hydroxyl radical scavenger to mimic the presence of organic compounds in a cellular system [58]. The

copper chloride and bromide complexes **1** and **5** did not have sufficient water solubility to perform these DNA damage studies.

$$Cu^{+} + H_2O_2 \rightarrow Cu^{2+} + {}^{\bullet}OH + OH^{-} \qquad (1)$$

DNA damage caused by increasing concentrations of complex **9** with H_2O_2 is shown in Figure 11. Lane 2 shows that hydrogen peroxide alone does not result in DNA damage, but reducing Cu^{2+} with ascorbate to form Cu^{+} in the presence of H_2O_2 results in DNA damage (lane 3, positive control). Upon adding increasing concentrations of complex **9**, DNA damage is significantly increased, with ~90 % DNA damage at 50 μM. Clotri alone does not damage DNA at these concentrations (data not shown), and uncoordinated Cu^{+} generated from $CuSO_4$ causes ~90% DNA damage at only 6 μM (lane 3), indicating that complex **9** remains largely intact under DNA damage assay conditions. Figure 12 shows a best-fit dose-response curve for DNA damage by complex **9**, with the concentration required to promote 50% DNA damage (EC_{50}) calculated as 10.47 ± 0.01 μM. Thus, $[Cu(clotri)_3NO_3]NO_3 \cdot 2H_2O$ (**9**) significantly promotes DNA damage, consistent with previous cytotoxicity studies [17].

DNA-adduct formation

Similar to cisplatin, DNA is believed to be the main target for this series of clotri coordination complexes [17]. For this reason, DNA from the HeLa human carcinoma cell line was isolated, and the amounts of Cu^{2+}, Co^{2+}, Zn^{2+}, and Ni^{2+} associated with this DNA were determined (Table 6). Cells treated with $[Cu(clotri)_2Br_2] \cdot 5H_2O$ (**5**) have the highest levels of DNA-associated metal (19.9 nmol $Cu^{2+}/10^6$ cells) followed by $[Cu(clotri)_2Cl_2] \cdot 5H_2O$ (**1**), $[Zn(clotri)_2Cl_2]$ (**3**), $[Co(clotri)_2Cl_2]$ (**2**), $[Ni(clotri)_3Br_2]$ (**8**), and $[Ni(clotri)_2Cl_2] \cdot H_2O$ (**4**) (13.4, 5.9, 5.5, 4.9 and 3.2 nmol $M^{2+}/10^6$ cells, respectively). The

amounts of M^{2+} found on the DNA of HeLa cells does not strictly correlate with the cytotoxicity or hydrophobicity (log P) of the complexes. However, it does correlate with the LD results where DNA association follows the decreasing order $Cu^{2+} > Zn^{2+} > Co^{2+}$. These data are also broadly consistent with the results of the EtBr displacement assay, where Cu^{2+} complexes generally showed higher affinity for DNA than Co^{2+} or Zn^{2+}. Overall, as suggested from the results presented herein, it is reasonable to assume that DNA is a potential target for these cytotoxic clotri-metal complexes.

Cytotoxicity

The obtained results correlate well with the previously published cytotoxicity data [17]. Cu^{2+} compounds **1** and **9** have been shown to exhibit generally lower IC_{50} values in HeLa growth studies compared with Co^{2+} complexes **2** and **10**. This finding correlates well with LD data suggesting that DNA interactions might be the cause of these compounds' cytotoxicity. The electrochemical results also correlate with the reported cytotoxicity, since Cu^{2+} complexes **1**, **5**, and **9** were the most cytotoxic clotri complexes [17], and these Cu^{2+} complexes readily undergo reduction to Cu^{+} ($Cu^{2+/+}$ potentials of -0.239 to -0.012 V). Cellular Cu^{+} is known to generate hydroxyl radical that causes DNA damage and death [59], and this reaction primarily occurs in biological systems if the metal redox potentials are between –0.324 to 0.460 V [60]. The less electrochemically accessible $Co^{3+/2+}$ potentials (0.512 V for the cobalt chloride complex **2** and only an oxidation potential of 0.977 V for the cobalt bromide complex **6**) lie outside the biological window for hydroxyl radical generation, so these complexes may be less likely to cause cellular damage by ROS formation. Unsurprisingly, the redox inactive Zn^{2+} complexes were found to be the least cytotoxic [9]. Correlation of the cellular toxicity results with the electrochemical redox

potentials for these complexes suggest that some of these compounds may cause cell death by generating ROS. Given the degree of DNA damage observed at relatively low concentrations of the copper complex **9**, it is likely that copper-mediated oxidative DNA damage is a significant part of the cytotoxicity.

Conclusions

DNA binding behavior of selected clotrimazole complexes was investigated using CD and LD spectroscopy, UV melting experiments, atomic force microscopy (AFM) and an ethidium bromide (EtBr) displacement assay. These results strongly suggest that the compounds bind to DNA in at least two different binding modes depending on the concentration, sequence of the DNA, and the structure of the complex. These results also show the dramatic effects that binding of these complexes has on the linear structure of the DNA. In addition, correlation of cytotoxicity data with the electrochemical redox potentials for these complexes also suggests that some of these compounds may cause cell death by generating ROS. The amounts of M^{2+} found on the DNA of human carcinoma cells did not correlate with the cytotoxic potency or hydrophobicity (log P) of the complexes. Overall, our results open wide possibilities for the design of complexes with not only desired cytotoxic activity, but also the capability of targeting specific DNA sequences. Such structural effects and, specifically, the ability to control and tune them are of high importance for the design of novel generations of metal-based anticancer complexes.

Acknowledgments

S.B.-L. thanks Dirección General de Asuntos del Personal Académico (DGAPA-UNAM) for funding. Financial support by Grants DGAPA-222713 and Conacyt CB2012-178851 is also acknowledged.

L.S. was financed by the MICINN of Spain with the Ramón y Cajal Fellowship RYC-2011-07787. The SGI/IZO-SGIker UPV/EHU is gratefully acknowledged for generous allocation of computational resources.

J.L.B. thanks the National Science Foundation grant CHE 1213912 for financial support.

Supporting information

Supporting information for this article can be found online.

References

1. L. Kelland, *Nat. Rev. Cancer*, 2007, **7**, 573–584.

2. D. Wang, S. J. Lippard, *Nat. Rev. Drug Discovery*, 2005, **4**, 307–320.

3. G. R. Zimmermann, J. Lehár, C.T. Keith, *Drug Discov. Today*, 2007, **12**, 34–42.

4. Z. Guo, P.J. Sadler, *Angew. Chem. Int. Ed.*, 1999, **38**, 1512–1531

5. Z. Guo, P.J. Sadler, *Adv. Inorg. Chem.*, 2000, **49**, 183–306.

6. E.E. Battin, J.L. Brumaghim, 2009, *Cell. Biochem. Biophys.*, **55**, 1–23.

7. V. Chagas da Silveira, J. Silva Luz, C. Columbano Oliveira, I. Graziani, M. R. Ciriolo, A. M. da Costa Ferreira, *J. Inorg. Biochem.*, 2008, **102**, 1090–1103.

8. J. Tan, B. Wang, L. Zhu, *J. Biol. Inorg. Chem.*, 2009, **14**, 727–739.

9. S. Kapitza, M. A. Jakupec, M. Uhl, B. K. Keppler, B. Marian, *Cancer Lett*., 2005, **226**, 115–121.

10. S. Betanzos-Lara, Z. Liu, A. Habtemariam, A.M. Pizarro, B. Qamar, P. J. Sadler, *Angew. Chem.*, 2012, **124**, 3963–3966.

11. Z. Liu, I. Romero-Canelón, B. Qamar, J. M. Hearn, A. Habtemariam, N. P. E. Barry, A. M. Pizarro, G. J. Clarkson, P. J. Sadler, *Angew. Chem. Int. Ed.*, 2014, **53**, 3941–3946.

12. Y. Fu, M. J. Romero, A. Habtemariam, M. E. Snowden, L. J. Song, G. J. Clarkson, B. Qamar, A. M. Pizarro, P. R. Unwin, P. J. Sadler, *Chem. Sci.*, 2012, **3**, 2485–2494.

13. V. Brabec, O. Novakova, *Drug Resist. Updates*, 2006, **9**, 111–122.

14. S. Betanzos-Lara, O. Novakova, R. J. Deeth, A. M. Pizarro, G. J. Clarkson, B. Liskova, V. Brabec, P. J. Sadler, A. Habtemariam, *J. Biol. Inorg. Chem.*, 2012, **17**, 1033–1051.

15. V. Brabec, S. E. Howson, R. A. Kaner, R. M. Lord, J. Malina, R. M. Phillips, Abdallah Q. M. A., P. C McGowan, A. Rodger, P. Scott, *Chem. Sci.*, 2013, **4**, 4407–4416.

16. O. Sánchez-Guadarrama, H. López-Sandoval, F. Sánchez-Bartéz, I. Gracia-Mora, H. Höpfl, N. Barba-Behrens, *J. Inorg. Biochem*., 2009, **103**, 1204–1213.

17. S. Betanzos-Lara, C. Gómez-Ruiz, L. R. Barrón-Sosa, I. Gracia-Mora, M. Flores-Álamo, N. Barba-Behrens, *J. Inorg. Biochem*., 2012, **114**, 82–93.

18. R. Marrington, T. R. Dafforn, D. J. Halsall, A. Rodger, *Biophys. J.*, 2004, **87**, 2002–2012.

19. R. Marrington, T. R. Dafforn, D. J. Halsall, J. I. MacDonald, M. Hicks, A. Rodger, *Analyst*, 2005, **130**, 1608–1616.

20. L. H. Li, T. F. DeKoning, R. C. Kelly, W. C. Krueger, J. P. McGovren, G. E. Padbury, G. L. Petzold, T. L. Wallace, R. J. Ouding, M. D. Prairie, I. Gebhard, *Cancer. Res.*, 1992, **52**, 4904–4913.

21. R. D. Wells, J. E. Larson, R. C. Grant, B. E. Shortle, C. R. Cantor, *J. Mol. Biol.*, 1970, **54**, 465–497.

22. R. B. Inman, R. L. Baldwin, *J. Mol. Biol.*, 1962, **5**, 172–171.

23. A. J Bard, L. R. Faulkner, 2004, in Electrochemical Methods, Fundamentals and Applications; 2nd ed.; Wiley: New York, pp 286–293.

24. N. G. Connelly, W. E. Geiger, *Chem. Rev.*, 1996, **96**, 877–910.

25. R. P. Hertzberg, P. B. Dervan, *J. Am. Chem. Soc.*, 1982, **104**, 313–315.

26. R. S. Lloyd, C. W. Haidle, D. L. Robberson, *Biochemistry*, 1978, **17**, 1890–1896.

27. I. Horcas, R. Fernández, J. M. Gómez-Rodríguez, J. Colchero, J. Gómez-Herrero, A. M. Baro, *Rev. Sci. Instrum.*, 2007, **78**, 013705–013708.

28. M. J. Frisch, G. W. Trucks, H. B. Schlegel, G. E Scuseria, M. A. Robb, J. R. Cheeseman, G. Scalmani, V. Barone, B. Mennucci, G. A. Petersson, H. Nakatsuji, M. Caricato, X. Li, H. P. Hratchian, A. F. Izmaylov, J. Bloino, G. Zheng, J. L. Sonnenberg, M. Hada, M. Ehara, K. Toyota, R. Fukuda, J. Hasegawa, M. Ishida, T. Nakajima, Y. Honda, O. Kitao, H. Nakai, T. Vreven, J. J. A. Montgomery, J. E. Peralta, F. Ogliaro, M. Bearpark, E. B. J. J. Heyd, K. N. Kudin, V. N. Staroverov, R. Kobayashi, J. Normand, K. Raghavachari, A. Rendell, J. C. Burant, S. S. Iyengar, J. Tomasi, M. Cossi, N. Rega, J. M. Millam, M. Klene, J. E. Knox, J. B. Cross, V. Bakken, C. Adamo, J. Jaramillo, R. Gomperts, R. E. Stratmann, O. Yazyev, A. J. Austin, R. Cammi, C. Pomelli, J. W. Ochterski, R. L. Martin,

K. Morokuma, V. G Zakrzewski, G. A. Voth, P. Salvador, J. J. Dannenberg, S. Dapprich, A. D. Daniels, Ö. Farkas, J. B. Foresman, J. V. Ortiz, J. Cioslowski, D. J. Fox, Gaussian 09 (Revision B.01), Gaussian, Inc., Wallingford CT, 2009.

29. J. P. Perdew, K. Burke, M. Ernzerhof, *Phys. Rev. Lett*., 1996, **77**, 3865–3868.

30. P. J. Hay, W. R. Wadt, *J. Chem. Phys.*, 1985, **82**, 270–283.

31. A. D. McLean, G. S. Chandler, *J. Chem. Phys.*, 1980, **72**, 5639–5648.

32. P. Fuentealba, H. Preuss, H. Stoll, L. V. Szentpaly, *Chem. Phys. Lett.*, 1982, **89**, 418–422.

33. E. Borfecchia, C. Garino, L. Salassa, T. Ruiu, D. Gianolio, X. Zhang, K. Attenkofer, L. X. Chen, R. Gobetto, P. J. Sadler, C. Lamberti, *Dalton Trans.*, 2013, **42**, 6564–6571.

34. S. R. Collinson, M. Schröder, in Nickel: Inorganic & Coordination Chemistry in Encyclopedia of Inorganic Chemistry, John Wiley & Sons, Ltd., 2006.

35. H. F. VanBrocklin, A. Liu, M. J. Welch, J. P. O'Neil, J. A. Katzenellenbogen, Steroids, 1994, 59, 34–45.

36. D. J. Minick, J. H. Frenz, M. A. Patrick, D. A. Brent, *J. Med. Chem.*, 1988, **31**, 1923–1933.

37. C. Hansch, J. P. Bjorkroth, A. Leo, *J. Pharm. Sci.*, **1987**, *76*, 663–687.

38. A. V. Klein, T. W. Hambley, 2009, *Chem. Rev.*, **109**, 4911–492.

39. C. A. Rabik, M. E. Dolan, *Cancer Treat. Rev.*, 2007, **33**, 9–23.

40. S. Y. Loh, P. Mistry, L. R. Kelland, G. Abel, K. R. Harrap, *Br. J. Cancer*, 1992, **66**, 1109–1115.

41. S. P. Oldfield, M. D. Hall, J. A. Platts, *J. Med. Chem.*, 2007, **50**, 5227–5237.

42. A. Rodger, K. K. Patel, K. J. Sanders, M. Datt, C. Sacht, M. J. Hannon, *J. Chem. Soc. Dalton Trans.*, 2002, 3656–3663.

43. J. SantaLucia*, Proc. Natl. Acad. Sci.*, 1998, **95**, 1460–1465.

44. N. Brooks, J. A. Hartley, J. E. Simpson Jr, S. R. Wright, S. Woo, S. Centioni, M. D. Fontaine, T. E. McIntyre, M. Lee, *Bioorg. Med. Chem.*, 1997, **5**, 1497–1507.

45. C. C. Tsai, S. C. Jain, H. M. Sobell, *Proc. Natl. Acad. Sci.*, 1975, **72**, 628–632.

46. J. B. Lepecq, C. Paoletti, *J. Mol. Biol.*, 1967, **27**, 87–106.

47. B. Nordén, A. Rodger, T. Dafforn, , in *Linear Dichroism and Circular Dichroism: A Textbook on Polarized-Light Spectroscopy*, Royal Society of Chemistry, Cambridge, 2010.

48. S. E. Howson, A. Bolhuis, V. Brabec, G. J. Clarkson, J. Malina, A. Rodger, P. Scott, *Nat. Chem.*, 2012, **4**, 31–36.

49. M. J. Hannon, V. Moreno, M. J. Prieto, E. Moldrheim, E. Sletten, I. Meistermann, C. J. Isaac, K. J. Sanders, A. Rodger, *Angew. Chem. Int. Ed.*, 2001, **40**, 879–884.

50. I. A. Taylor, K. G. Davis, D. Watts, G. G. Kneale, *Embo. J.*, 1994, **13**, 5772–5778.

51. C. M. Araujo, M. D. Doherty, S. J. Konezny, O. R. Luca, A. Usyatinsky, H. Grade, E. Lobkovsky, G. L. Soloveichik, R. H. Crabtree, V. S. Batista, *Dalton Trans.,* 2012, **41**, 3562–3573.

52. M. A. Neelakantan, M. Sundaram, M. S. Nair, *J. Chem. Eng. Data*, 2011, **56**, 2527–2535.

53. D. M. Boghaei, S. S. Farvid, M. Gharagozlou, *Spectrochim. Acta*, 2007, **A66**, 650–655.

54. A. P. Brown, F. C. Anson, *Anal. Chem.*, 1977, **49**, 1589–1595

55. M. M. Kimani, J. L. Brumaghim, D. Vanderveer, *Inorg. Chem.*, 2010, **49**, 9200–9211.

56. R. Miyamoto, R. Santo, T. Matsushita, T. Nishioka, A. Ichimura, Y. Teki, I. Kinoshita, *Dalton Trans.*, 2005, 3179–3186.

57. C. Angelé-Martínez, C. Goodman, J. L. Brumaghim, *Metallomics*, 2014, **6**, 1358–1381.

58. J.A. Imlay, S. Linn, *Science*, 1988, **240**, 1302-1309.

59. D. C. Ramírez, S. E. Gómez Mejiba, R. P. Mason, *J. Biol. Chem.*, **2005**, 280, 27402–27411.

60. J. L. Pierre, M. Fontecave, *BioMetals*, 1999, **12**, 195–199.

Table 1. Selected calculated bond distances (Å) and angles (°) for complexes **1–7**.

Bond distances (Å)	**(1) M = Cu^{2+}**	**(2) M = Co^{2+}**	**(3) M = Zn^{2+}**	**(3) X-ray***	**(4) M = Ni^{2+}**
M–Cl(1)	2.348(2)	2.323(8)	2.331(8)	2.210(6)	2.331(9)
M–Cl(2)	2.340(0)	2.339(0)	2.357(3)	2.222(9)	2.329(6)
M–N(1)	1.988(2)	2.048(1)	2.112(7)	2.043(7)	2.021(8)
M–N(2)	1.986(9)	2.050(4)	2.114(4)	2.060(1)	2.021(8)
Bond angles (°)					
Cl(1)–M–Cl(2)	142.5(8)	118.4(4)	126.8(6)	114.5(6)	146.2(8)
Cl(1)–M–N(1)	94.1(9)	109.7(3)	109.8(5)	108.9(0)	100.6(1)
Cl(1)–M–N(2)	94.6(5)	109.3(8)	107.6(4)	115.8(3)	100.7(8)
Cl(2)–M–N(1)	94.6(9)	103.2(5)	102.5(7)	113.4(5)	101.2(0)
Cl(2)–M–N(2)	93.7(7)	106.2(8)	104.2(4)	103.8(0)	101.0(3)
N(1)–M–N(2)	152.7(8)	109.3(8)	103.3(2)	99.3(7)	98.5(5)
Bond distances (Å)	**(5) M = Cu^{2+}**	**(6) M = Co^{2+}**	**(7) M = Zn^{2+}**	**(7) X-ray***	
M–Br(1)	2.475(4)	2.44751	2.471(6)	2.343(2)	
M–Br(2)	2.464(6)	2.45589	2.483(6)	2.361(1)	
M–N(1)	1.989(1)	2.04538	2.110(0)	2.036(7)	
M–N(2)	1.989(0)	2.04945	2.105(6)	2.039(1)	
Bond angles (°)					
Br(1)–M–Br(2)	137.4(4)	116.4(2)	126.0(6)	112.7(5)	
Br(1)–M–N(1)	95.7(2)	110.0(0)	107.7(2)	103.6(7)	
Br(1)–M–N(2)	95.7(3)	105.0(9)	104.7(8)	114.4(1)	
Br(2)–M–N(1)	95.0(0)	104.3(6)	103.7(0)	117.3(2)	
Br(2)–M–N(2)	94.9(8)	110.5(7)	106.0(9)	108.5(4)	
N(1)–M–N(2)	150.1(8)	110.4(4)	107.3(9)	99.6(3)	

* From reference 17

Table 2. The log P and IC_{50} values for complexes **1**–**4**, **6**, **8** and **9** log P values are the mean of two independent experiments and are expressed as mean ± SD.

		log P		IC_{50} (μM)
	Compound	**Mean**	**SD**	**HeLa**
(**1**)	$[Cu(clotri)_2Cl_2]\cdot 5H_2O$	–0.62	0.02	6.8
(**2**)	$[Co(clotri)_2Cl_2]$	–0.43	0.02	7.0
(**3**)	$[Zn(clotri)_2Cl_2]$	–0.27	0.09	7.1
(**4**)	$[Ni(clotri)_2Cl_2]\cdot H_2O$	–1.95	0.17	8.1
(**6**)	$[Co(clotri)_2Br_2]$	–1.14	0.10	20.6
(**8**)	$[Ni(clotri)_3Br_2]$	–2.09	0.06	13.6
(**9**)	$[Cu(clotri)_3NO_3]NO_3\cdot 2H_2O$	–0.28	0.05	3.5
	Clotrimazole	5.44	0.51	12.4
	Cisplatin	–2.30		5.2

Table 3. Apparent DNA-binding constants, K_{app} ($\times 10^4$ M^{-1}), for clotri metal complexes **1**–**3** and **9**–**10**. K_{app} values are the mean of two independent experiments and are expressed as mean ± SD.

	Compound	ct-DNA	poly(dA-dT)$_2$	poly(dG-dC)$_2$
(**1**)	$[Cu(clotri)_2Cl_2]\cdot 5H_2O$	4.9 ± 0.5	6.4 ± 0.2	6.81 ± 0.09
(**2**)	$[Co(clotri)_2Cl_2]$	4.7 ± 0.2	5.47 ± 0.09	5.6 ±-0.7
(**3**)	$[Zn(clotri)_2Cl_2]$	4.9 ± 0.4	5.23 ± 0.08	5.90 ± 0.04
(**9**)	$[Cu(clotri)_3NO_3]NO_3\cdot 2H_2O$	6.2 ±0.1	6.2 ± 0.3	6.45 ±0.03
(**10**)	$[Co(clotri)_3(NO_3)_2]$	6.7 ±0.4	6.2 ± 0.2	7.0 ± 0.7

Table 4. The calculated concentrations of complexes **1–3** and **9–10** at which 50% loss of LD signal was recorded (K_a, μM)

	Compound	K_a (μM)
(**1**)	$[Cu(clotri)_2Cl_2]\cdot 5H_2O$	40 ± 1
(**2**)	$[Co(clotri)_2Cl_2]$	70 ± 2
(**3**)	$[Zn(clotri)_2Cl_2]$	51 ± 4
(**9**)	$[Cu(clotri)_3NO_3]NO_3\cdot 2H_2O$	55 ± 2
(**10**)	$[Co(clotri)_3(NO_3)_2]$	80 ± 1

Table 5. Electrochemical potentials (versus NHE) from cyclic voltammetry studies of clotri complexes **1**–**2**, **5**–**7**, and **9**–**10** in acetonitrile.

Compound	Ep_a (V)	Ep_c (V)	ΔE (V)	$E_{1/2}$ (V)
(**1**) $[Cu(clotri)_2Cl_2]\cdot 5H_2O$	-0.512[d], -0.082[e]	-1.192[d], -0.379[e]	0.680[d], 0.297[e]	-0.852[d], -0.239[e]
(**2**) $[Co(clotri)_2Cl_2]$	-0.238[b], 0.997[c], 1.206[a]	—	—	—
(**5**) $[Cu(clotri)_2Br_2]\cdot 5H_2O$	-0.479[d], 0.018[e], 0.962[a]	-1.407[d], -0.297[e], 0.614[a]	0.928[d], 0.279[e], 0.348[a]	-0.943[d], -0.139[e], 0.788[a]
(**6**) $[Co(clotri)_2Br_2]$	-0.038[b], 0.648[c], 0.948[a]	-1.612[b], 0.376[c],0755[a]	1.574[b], 0.272[c], 0.193[a]	-0.825[b], 0.512[c], 0852[a]
(**7**) $[Zn(clotri)_2Br_2]$	1.021[a]	0.591[a]	0.435[a]	0.806[a]
(**9**) $[Cu(clotri)_3NO_3][NO_3]\cdot 2H_2O$	-0.441[d], 0.117[e], 0.693[a]	-1.603[d], -0.141[e], 0.338[a]	1.162[d], 0.258[e], 0.355[a]	-1.022[d], -0.012[e], 0.515[a]
(**10**) $[Co(clotri)_3(NO_3)_2]$	-0.296[b]	-1.669[b]	1.373[b]	-0.982[b]

[a]Clotri ligand potentials; [b]$Co^{2+/0}$ potentials; [c]$Co^{3+/2+}$ potentials; [d]$Cu^{+/0}$ potentials; [e]$Cu^{2+/+}$ potentials.

Table 6. DNA metal concentration of metal ion for complexes **1**–**5** and **8** in HeLa human carcinoma cell line ($nM^{2+}/10^6$ cells).

	Compound	DNA binding ($nM\ M^{2+}/10^6$ cells)
(**1**)	$[Cu(clotri)_2Cl_2]\cdot 5H_2O$	13.4
(**2**)	$[Co(clotri)_2Cl_2]$	5.5
(**3**)	$[Zn(clotri)_2Cl_2]$	5.9
(**4**)	$[Ni(clotri)_2Cl_2]\cdot H_2O$	3.2
(**5**)	$[Cu(clotri)_2Br_2]\cdot 5H_2O$	19.9
(**8**)	$[Ni(clotri)_3Br_2]$	4.9

Figure Captions

Figure 1. General structures of the Cu^{II}, Co^{II}, Zn^{II}, and Ni^{II} complexes of clotrimazole (clotri) studied in this work.

Figure 2. Electrostatic Potential Surfaces (EPS) for complexes **1–4** shown in both space and mapped on the electron density (isovalue 0.001) of molecules. The electrostatic potential is represented with a color scale going from red (–0.1 au) to blue (0.1 au).

Figure 3. Effects of clotri complexes **1–3** and **9–10** on thermal stability of ct-DNA at 20:1, 10:1 and 5:1 (DNA bp:compound) ratios.

Figure 4. Ethidium bromide displacement titration of ct-DNA with $[Cu(clotri)_2Cl_2]\cdot 5H_2O$ (**1**). The inset shows decreasing fluorescence at 585 nm. See weak shoulder at 620 nm for higher concentrations of **1**, due to intrinsic florescence of this compound.

Figure 5. Left: Linear dichroism (LD) spectra of 100 μM DNA with increasing concentration of $[Cu(clotri)_2Cl_2]\cdot 5H_2O$ (**1**). Right: The resulting titration curve at 260 nm.

Figure 6. Left: LD spectrum of ct-DNA in the presence of $[Cu(clotri)_2Cl_2]\cdot 5H_2O$ (**1**) (black line) and an overlaid LD spectrum on ct-DNA scaled to the same intensity (red line). Additional bands can be seen at indicated wavelengths. Right: The calculated LD spectrum of $[Cu(clotri)_2Cl_2]\cdot 5H_2O$ (**1**) bound to DNA (black) and an overlaid UV spectrum of $[Cu(clotri)_2Cl_2]\cdot 5H_2O$ (**1**) (red and blue, not to scale).

Figure 7. LD signal of DNA at 260 nm with increasing concentration of $[Co(clotri)_3(NO_3)_2]$ (**10**) showing a two-step binding process.

Figure 8. CD spectra of 50 μM DNA with increasing concentrations of complex $[Zn(clotri)_2Cl_2]$ (**3**).

Figure 9. TM-AMF images of linearized pUC19 plasmid DNA with increasing concentrations of $[Cu(clotri)_2Cl_2]$ (**1**). a) DNA only, b) 10:1 DNA:**1**, c) 10:3 DNA:**1** and d) 10:5 DNA:**1**.

Figure 10. Cyclic voltammograms vs NHE for A) $[Cu(clotri)_2Cl_2]\cdot 5H_2O$ (**1**), B) $[Cu(clotri)_2Br_2]\cdot 5H_2O$ (**5**), and C) $[Cu(clotri)_3NO_3]NO_3\cdot 2H_2O$ (**8**) at 1 mM in CH_3CN with 0.1 M $TBAPF_6$ as the supporting electrolyte.

Figure 11. Cyclic voltammograms of A) $[Cu(clotri)_2Cl_2]\cdot 5H_2O$ and B) $[Cu(clotri)_2Br_2]\cdot 5H_2O$ at 1 mM in dichloromethane with 0.1 M $TBAPF_6$ as the supporting electrolyte.

Figure 12. Gel electrophoresis image of Cu^+-mediated DNA damage by $[Cu(clotri)_3NO_3][NO_3]\cdot 2H_2O$ (**9**) in MOPS buffer (10 mM, pH 7). Lanes: MW = 1 kb molecular weight marker; lane 1: plasmid DNA (p); lane 2: p + H_2O_2; lane 3: p + ascorbate (7.5 μM) + $CuSO_4$ (6 μM) + H_2O_2 (50 μM); lanes 4-18: p + increasing compound concentration + ascorbate + H_2O_2: 1 (lanes 4-6), 5 (lanes 7-9), 10 (lanes 10-12), 25 (lanes 13-15), and 50 μM (lanes 16-18) $[Cu(clotri)_3NO_3][NO_3]\cdot 2H_2O$ (**9**) respectively.

Figure 13. Best-fit dose-response curve for percent DNA damage versus concentration for $[Cu(clotri)_3NO_3][NO_3]\cdot 2H_2O$ (**9**).

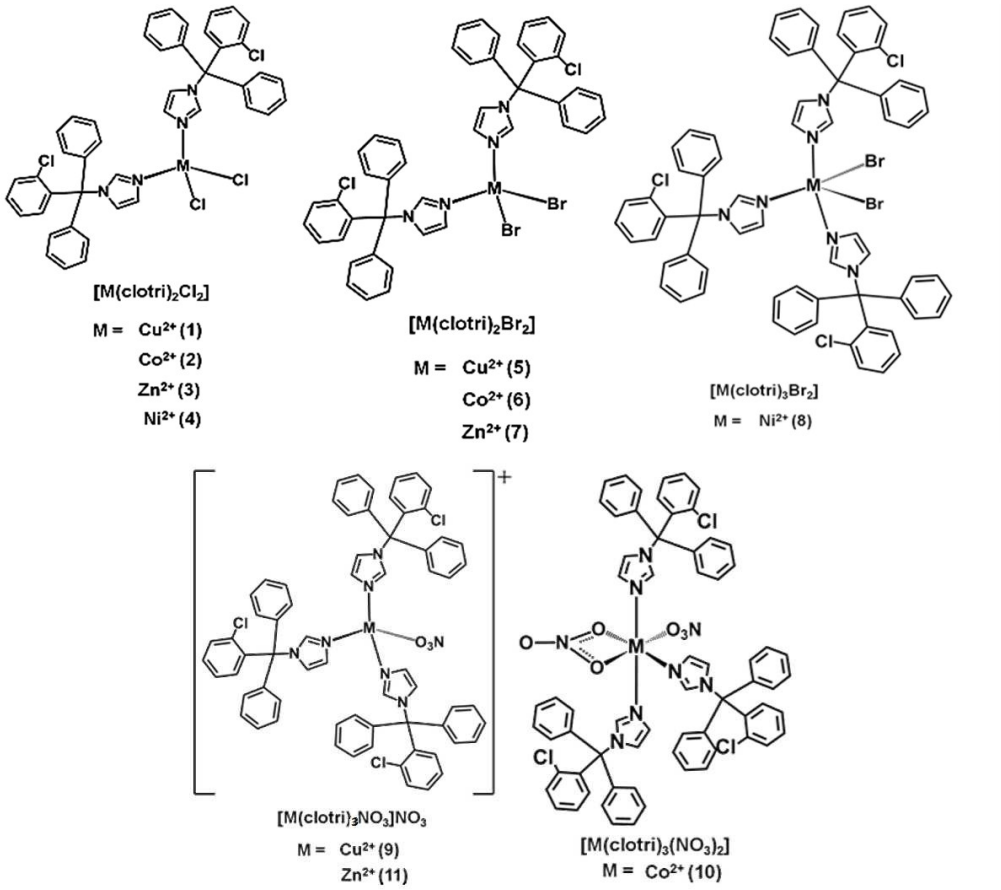

Figure 1.

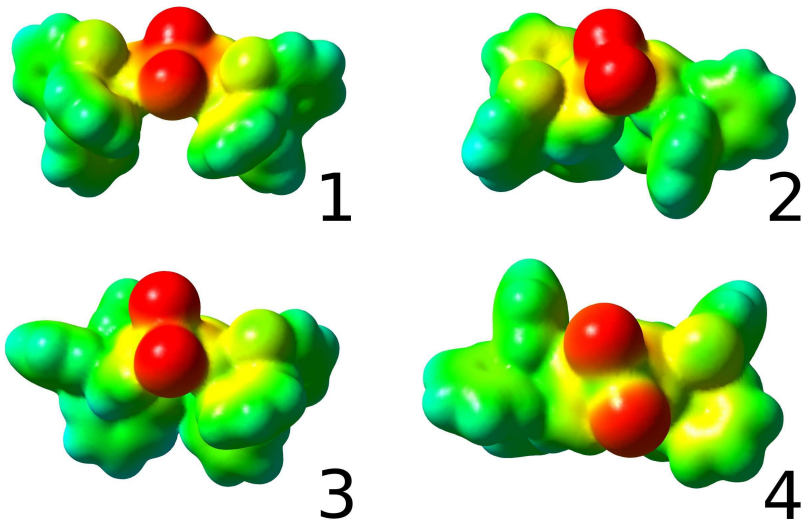

Figure 2.

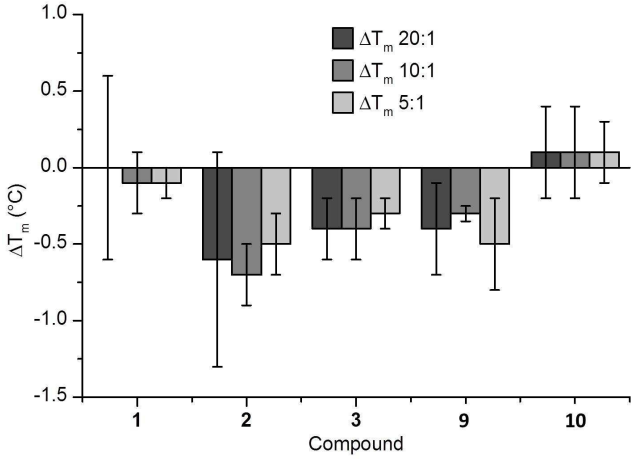

Figure 3.

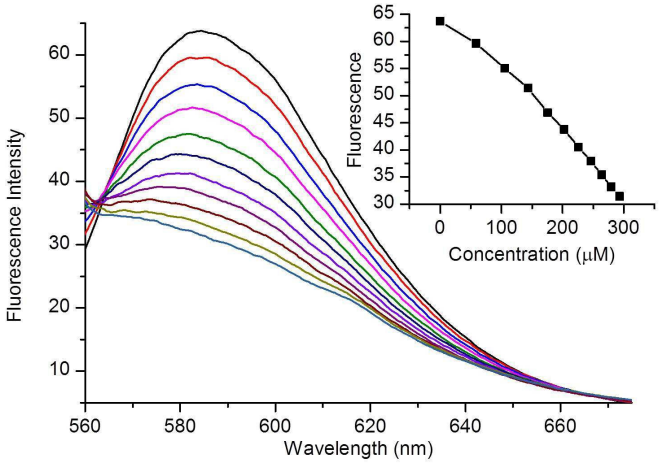

Figure 4.

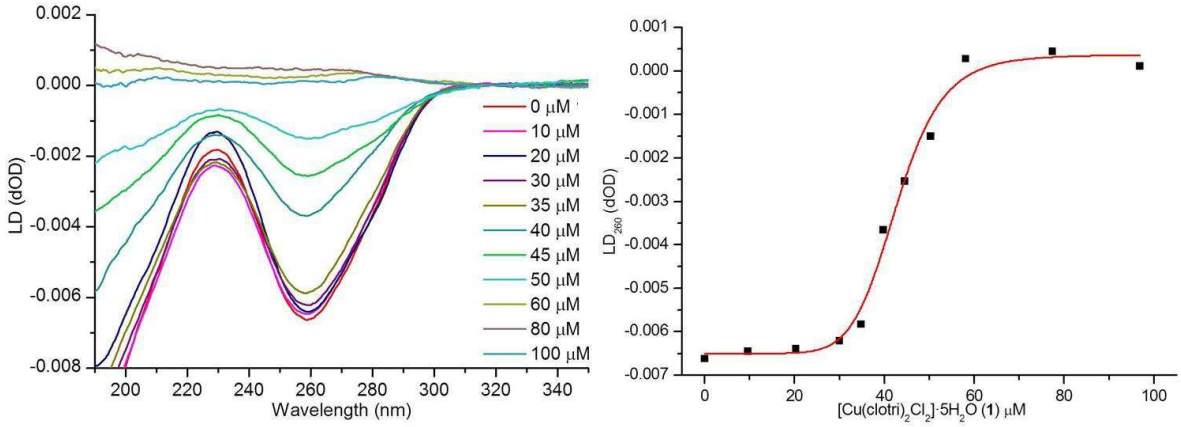

Figure 5.

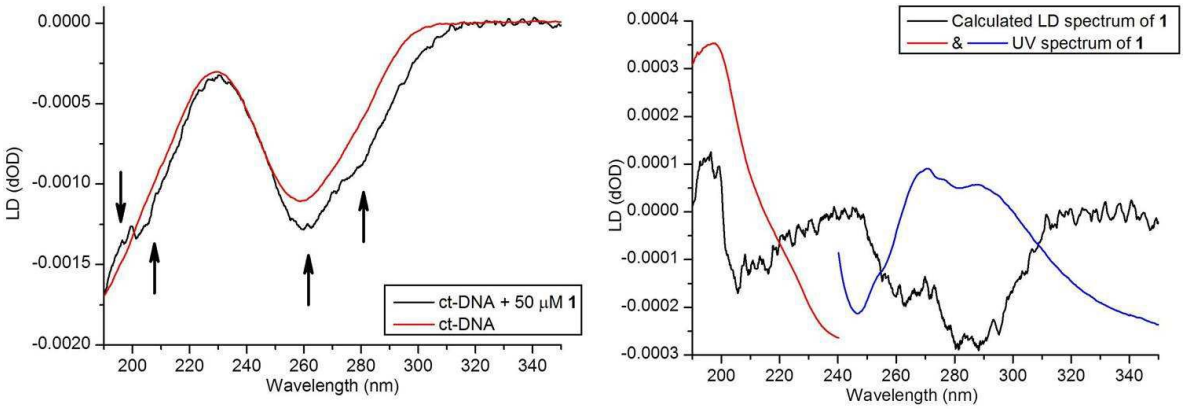

Figure 6.

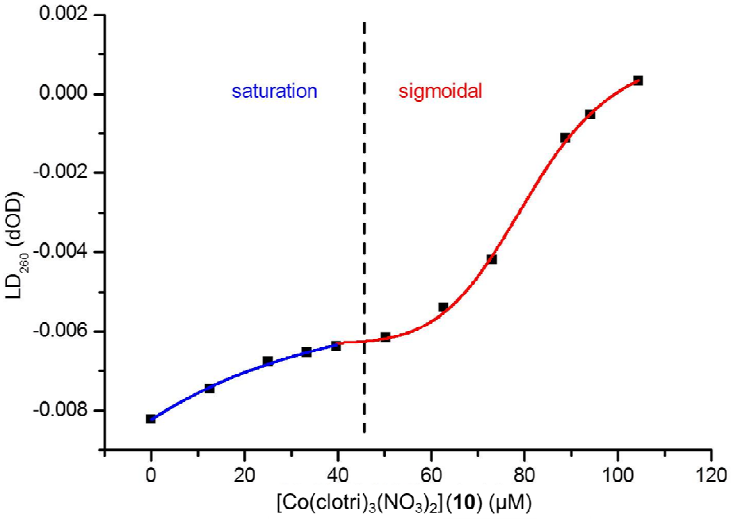

Figure 7.

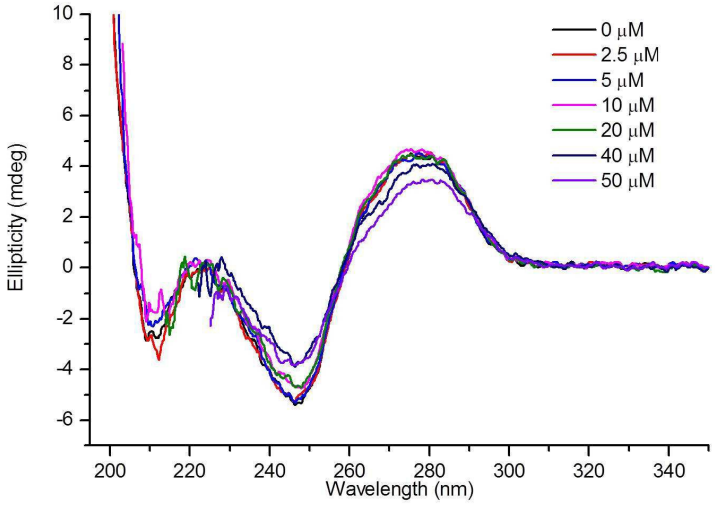

Figure 8.

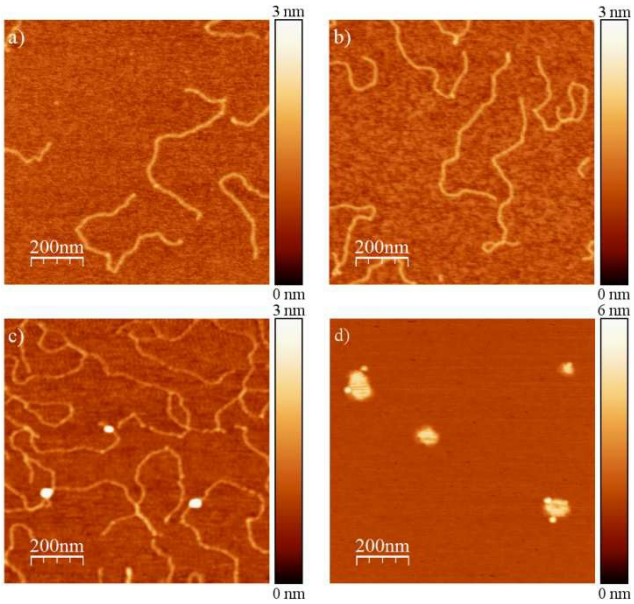

Figure 9.

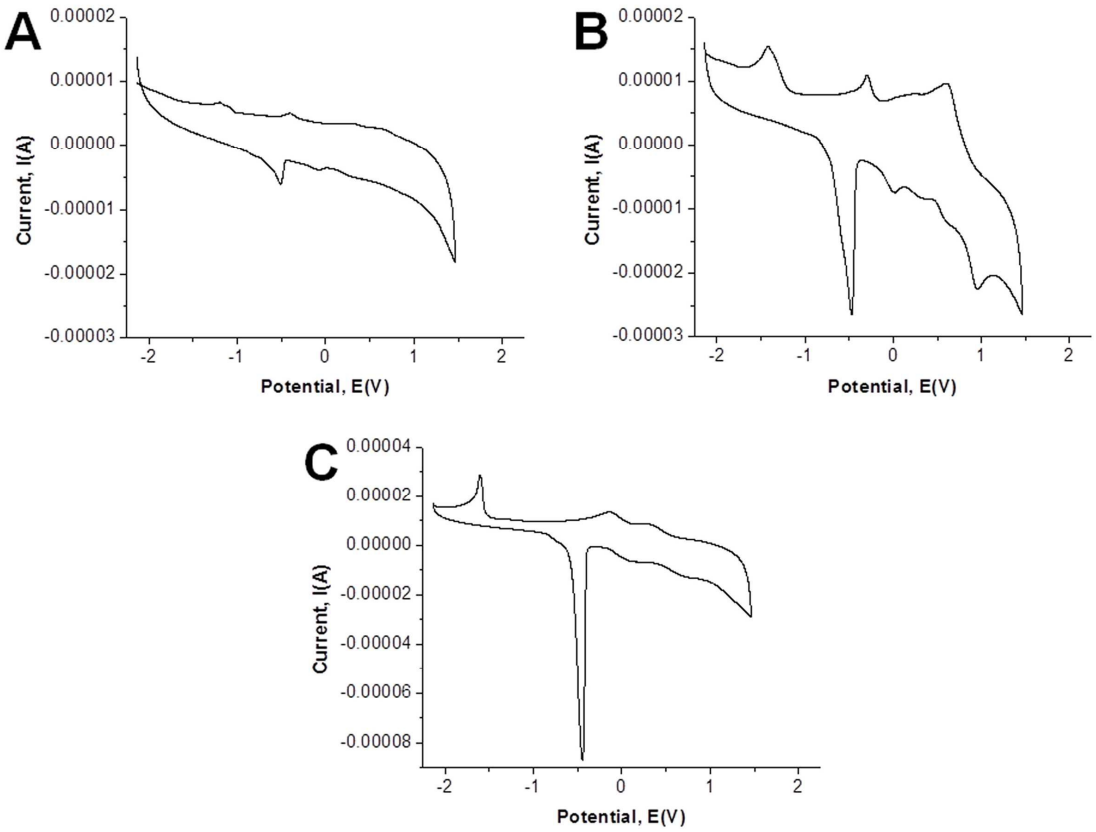

Figure 10.

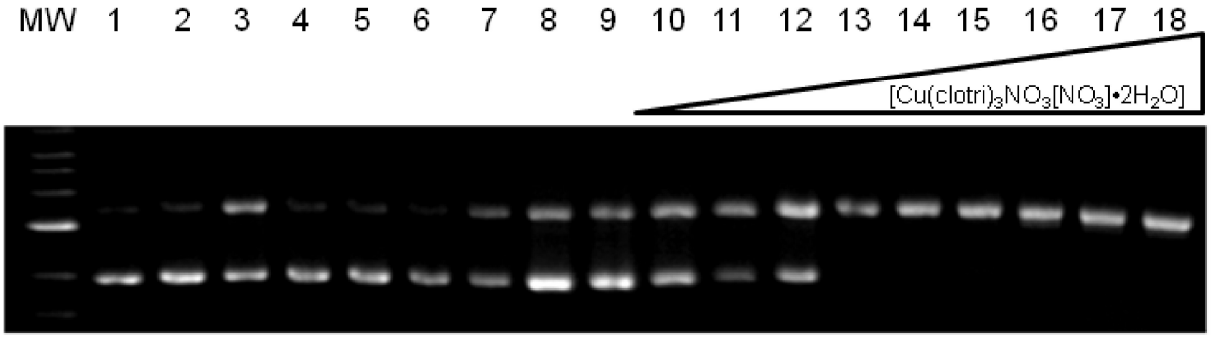

Figure 11.

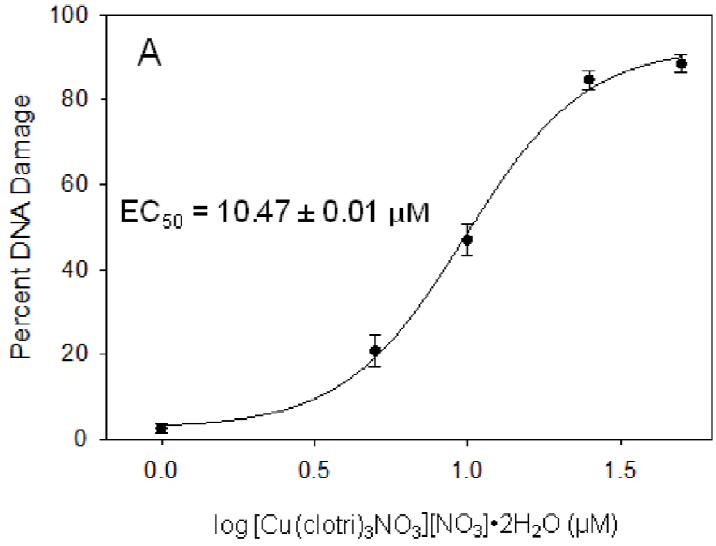

Figure 12.

Redox-active and DNA-binding coordination complexes of clotrimazole

Soledad Betanzos-Lara, Nikola P. Chmel, Matthew T. Zimmerman, Lidia R. Barrón-Sosa, Claudio Garino, Luca Salassa, Alison Rodger, Julia Brumaghim, Isabel Gracia-Mora and Noráh Barba-Behrens

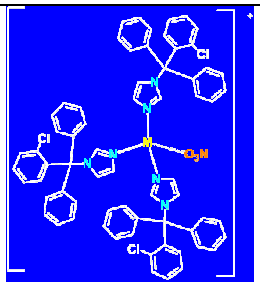

The coordination compounds bind to DNA by two different binding modes depending on the concentration, sequence of the DNA, and the structure of the complex. Cytotoxicity data and electrochemical redox potentials show that some of these compounds may cause cell death by generating ROS. Structural effects, and the ability to control and tune them, are of importance for the design of novel metal-based anticancer complexes.